Annals of Nuclear Medicine Vol. 19, No. 7, 589–595, 2005

An experimental study on *O*-[^{18}F]fluoromethyl-L-tyrosine for differentiation between tumor and inflammatory tissues

Manami SUZUKI,* Keiichiro YAMAGUCHI,** Go HONDA,* Ren IWATA,*** Shozo FURUMOTO,**** Myeong-gi JEONG,* Hiroshi FUKUDA***** and Masatoshi ITOH*

*Division of Nuclear Medicine, Cyclotron and Radioisotope Center, Tohoku University
**Department of Radiology, Sendai Kousei Hospital
***Division of Radiopharmaceutical Chemistry, Cyclotron and Radioisotope Center, Tohoku University
****Biomedical Engineering Research Organization, Tohoku University
*****Division of Nuclear Medicine and Radiology, Institute of Development, Aging and Cancer, Tohoku University

Objective: *O*-[^{18}F]fluoromethyl-L-tyrosine (^{18}F-FMT) is a recently developed tumor-detecting agent with simple preparation and high radiochemical yields. The aim of this study was to assess the potency of ^{18}F-FMT for differentiating tumor and inflammatory tissues using an animal model with an implanted tumor and experimentally induced inflammatory foci. ***Methods:*** An ascites hepatoma cell line, AH109A, turpentine oil and *Staphylococcus aureus* were inoculated subcutaneously into Donryu rats as a tumor model, aseptic inflammation model and bacterial infection model, respectively. The biodistribution of radioactivity was assessed in rats at 5, 10, 30, 60, and 120 min after injection with ^{18}F-FMT. Dual tracer whole-body and macro autoradiographies were performed 60 min after injection with a mixture of ^{18}F-FMT and 2-deoxy-D-[1-^{14}C]glucose (^{14}C-DG). ***Results:*** Tumor uptake of ^{18}F-FMT was on average 1.27% injected dose per gram of tissue (%ID/g) and 1.43%ID/g at 30 min and 60 min, respectively and significantly higher than that in other normal tissues, except the pancreas (3.48%ID/g at 60 min). The uptakes in the aseptic and bacterial inflammatory tissues were very low and were not different from those of the background tissues. Dual tracer whole-body and macro autoradiographic studies showed that tumor uptake of ^{18}F-FMT was clearly higher than uptake by the other tissues, while ^{18}F-FMT accumulated much less both in aseptic and bacterial inflammatory tissues. In contrast, the ^{14}C-DG images showed high accumulations not only in tumors but also in aseptic and bacterial inflammatory tissues. ***Conclusion:*** ^{18}F-FMT seems to be a promissing tracer for the differentiation between tumor and inflammation because of higher specificity to tumor.

Key words: *O*-[^{18}F]fluoromethyl-L-tyrosine, 2-deoxy-D-[1-^{14}C]glucose, ^{18}F-FDG, tumor, inflammation

INTRODUCTION

THE GLUCOSE ANALOG, ^{18}F-2-deoxy-2-fluoro-D-glucose (^{18}F-FDG), is widely used as a tumor-detecting agent. Positron emission tomography (PET) studies with ^{18}F-FDG have demonstrated its usefulness in clinical oncology practice.[1,2] However, ^{18}F-FDG accumulates highly not only in tumor but also in inflammation.[3–6] This nonspecific accumulation of ^{18}F-FDG leads to false-positive results and reduces diagnostic specificity.[7] Several methods to increase the contrast between tumor and inflammation have been proposed for ^{18}F-FDG-PET, i.e., dual-time-point ^{18}F-FDG-PET imaging,[8] delayed ^{18}F-FDG-PET imaging,[9] and insulin and glucose loading.[10] However, all of these methods have had limited success.

In tumor cells, amino acid metabolism is enhanced, and amino acid transport and the rate of protein synthesis increase.[11–13] On the other hand, inflammatory cells do

Received January 21, 2005, revision accepted August 1, 2005.
For reprint contact: Manami Suzuki, M.D., Division of Nuclear Medicine, Cyclotron and Radioisotope Center, Tohoku University, Aoba, Aramaki, Aoba, Sendai, Miyagi 980–8578, JAPAN.
E-mail: manami@cyric.tohoku.ac.jp

not take up amino acids much, compared with ^{18}F-FDG.[14–16] These properties suggest possible advantages of amino acid tracers over ^{18}F-FDG in tumor imaging at least with respect to the specificity. Various amino acids have been labeled for tumor detection and investigated for their clinical efficacy in oncology.[17,18]

^{18}F-labeled tyrosine analogs such as *O*-(2-[^{18}F]fluoroethyl)-L-tyrosine (^{18}F-FET),[19–21] L-3-[^{18}F]fluoro-α-methyl tyrosine[22,23] and 2-[^{18}F]fluoro-L-tyrosine,[24] have been developed. Recently, the synthesis of *O*-[^{18}F]fluoromethyl-L-tyrosine (^{18}F-FMT), has been reported as a new tumor-detecting agent by Iwata et al.[25] The preparation of ^{18}F-FMT was simple with high radiochemical yields and consequently suitable for routine production.

The aim of this study was to assess the potency of ^{18}F-FMT for the differentiation between tumor and inflammatory tissues using animal models with implanted tumor and experimentally induced aseptic and bacterial inflammatory tissues, in comparison with 2-deoxy-D-[1-^{14}C]glucose (^{14}C-DG).

MATERIALS AND METHODS

The animal studies were carried out following the guidelines and with the permission of the Animal Ethical Committees of the Cyclotron and Radioisotope Center, Tohoku University.

The methods of ^{18}F-FMT labeling with ^{18}F were reported elsewhere.[25] Briefly, ^{18}F-FMT was labeled by reacting trifluoromethyloxy triflate, a highly reactive labeling intermediate, with tyrosine disodium salt in DMSO at room temperature. Radiochemical yield was from 75 to 87%, with an overall yield of 30–40%. The overall synthesis time including HPLC purification was about 50 min.

Animal model

Male Donryu rats weighing 200 to 250 g (Japan SLC, Japan) were used. They were fed food and water ad libitum. An ascites hepatoma cell line, AH109A (Cell Resource Center for Biomedical Research, Institute of Development, Aging and Cancer, Tohoku University, Japan) was used as a tumor model. The cells had been maintained in the ascetic form by intermittent intraperitoneal inoculations. AH109A cells of 5×10^6 were inoculated subcutaneously into the left thigh of the rats 7 days before the experiment. Ten microliters of turpentine oil (Wako Pure Chemical Industries Co., Ltd., Japan) was inoculated subcutaneously into the back of the same rat twice in different locations 12 and 4 days before the experiment (Day 12 and 4) to induce aseptic inflammation. Bacterial inflammation was induced with subcutaneous inoculation of 0.1 m*l* of the suspension of *Staphylococcus aureus* (*S. aureus*) into the right thigh of the rats 3 days before the experiment. A suspension of *S. aureus* was prepared in sterile saline (1×10^9 CFU/m*l*) according to the optical density determination based on the standard curve obtained in the preliminary experiment.

Histological examination of inflammatory tissues

Histological examination was performed in a separate rat, bearing both aseptic and bacterial inflammatory foci induced as above. The inflammation was confirmed microscopically with hematoxylin-eosin (HE) stain.

Biodistribution study of ^{18}F-FMT

Rats were injected intravenously with 1.85 MBq of ^{18}F-FMT in 0.2 m*l* saline via the tail vein, and sacrificed by cervical dislocation at 5, 10, 30, 60 and 120 min after injection. The tumor, aseptic inflammation, bacterial inflammation, blood, brain, heart, lung, pancreas, liver, kidney, small intestine, muscle, bone, and urine were partially or totally dissected immediately. The samples were weighed and ^{18}F radioactivities were measured with a gamma counter (PerkinElmer, Inc., USA). The tissue uptake except for the urine was expressed as a percentage of the injected dose per gram of tissue (%ID/g). The radioactivity in the urine was expressed as a percentage of the injected dose (%ID).

Dual tracer whole-body autoradiography

A rat bearing both AH109A and two aseptic inflammatory foci with turpentine oil (Day 12 and 4) was injected with a mixture of 74 MBq of ^{18}F-FMT and 185 kBq of ^{14}C-DG (American Radiolabeled Chemicals, Inc., USA) via the tail vein, and was sacrificed with an overdose of diethyl ether anesthesia at 60 min after injection. The rat was embedded in 3% solution of carboxymethylcellulose sodium salt (Wako Pure Chemical Industries Co., Ltd., Japan) and was frozen in acetone-dry ice (–80°C). Fifty-micrometer-thick rat sections were obtained with a cryotome (Nakagawa Seisakusho Co., Ltd., Japan) at –20°C and were collected on adhesive tape (Nakagawa Seisakusho Co., Ltd., Japan). The sections were exposed to the imaging plate (BAS-SR2025, Fuji Photo Film Co., Ltd., Japan) at –20°C for 45 min to produce ^{18}F-FMT images. The same samples were exposed to another imaging plate again for 7 days to generate ^{14}C-DG images, 4 days after the first exposure. Autoradiograms were digitized using the Bio-Imaging Analyzer (BAS-5000, Fuji Photo Film Co., Ltd., Japan).

Dual tracer macro autoradiography

Two rats bearing AH109A tumor, two aseptic inflammatory foci induced by turpentine oil (Day 12 and 4) and a bacterial inflammatory focus induced by *S. aureus* were injected intravenously with a mixture of 18.5 MBq of ^{18}F-FMT and 185 kBq of ^{14}C-DG via the tail vein, and sacrificed 60 min after injection. Tumor, aseptic and bacterial inflammatory tissues and the muscle were dissected immediately, and each of them was embedded in

Table 1 Tissue distributions of ^{18}F-FMT in rats with AH109A tumor and aseptic and bacterial inflammation

Tissue	Time after injection				
	5 min	10 min	30 min	60 min	120 min
Tumor	0.64 ± 0.31	0.78 ± 0.41	1.27 ± 0.35	1.43 ± 0.43	1.06 ± 0.37
Day 4 aseptic inflammation	0.49 ± 0.07	0.43 ± 0.10	0.50 ± 0.08	0.50 ± 0.13	0.59 ± 0.11
Day 12 aseptic inflammation	0.46 ± 0.21	0.41 ± 0.11	0.53 ± 0.14	0.50 ± 0.14	0.64 ± 0.22
Bacterial inflammation	0.62 ± 0.05	0.59 ± 0.07	0.61 ± 0.05	0.59 ± 0.08	0.59 ± 0.09
Blood	0.63 ± 0.10	0.51 ± 0.10	0.51 ± 0.09	0.46 ± 0.09	0.48 ± 0.08
Brain	0.36 ± 0.12	0.37 ± 0.11	0.52 ± 0.12	0.47 ± 0.12	0.46 ± 0.11
Heart	0.56 ± 0.08	0.48 ± 0.11	0.46 ± 0.07	0.41 ± 0.09	0.44 ± 0.06
Lung	0.55 ± 0.14	0.46 ± 0.08	0.45 ± 0.08	0.41 ± 0.09	0.42 ± 0.09
Pancreas	3.68 ± 1.15	3.15 ± 0.74	3.16 ± 0.52	3.48 ± 0.55	3.42 ± 0.47
Liver	0.59 ± 0.13	0.53 ± 0.15	0.45 ± 0.08	0.43 ± 0.08	0.43 ± 0.05
Kidney	0.65 ± 0.19	0.53 ± 0.12	0.48 ± 0.08	0.42 ± 0.07	0.42 ± 0.06
Small intestine	0.51 ± 0.19	0.42 ± 0.13	0.38 ± 0.09	0.41 ± 0.09	0.40 ± 0.08
Muscle	0.52 ± 0.17	0.45 ± 0.14	0.44 ± 0.09	0.43 ± 0.07	0.43 ± 0.09
Bone	0.38 ± 0.13	0.39 ± 0.11	0.39 ± 0.07	0.51 ± 0.11	0.62 ± 0.11
Urine*	—	0.41 ± 0.36	1.56 ± 1.39	1.79 ± 1.17	3.31 ± 1.37

Values are expressed as mean ± S.D. of %ID/g. (n = 8)
*Values are expressed as mean ± S.D. of %ID. (n = 4)

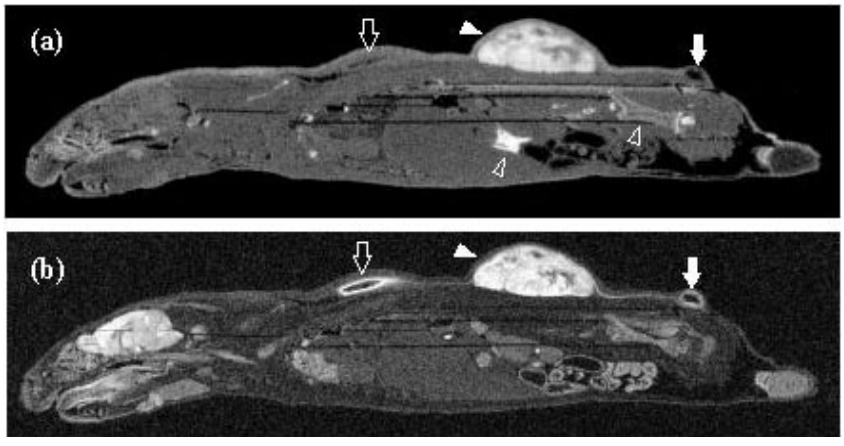

Fig. 1 Whole-body autoradiograms of a rat with experimentally induced aseptic inflammation and an implanted tumor. The ^{18}F-FMT image (a) and ^{14}C-DG image (b) are shown. Closed arrow, closed arrowhead and open arrow on the back (from caudal to cranial) show Day 12 aseptic inflammation, AH109A tumor and Day 4 aseptic inflammation, respectively. The open arrowheads in the abdomen and lumbar regions (^{18}F-FMT only) correspond to the pancreas and the femur cortex respectively.

the mounting gel (Tissue-Tek, Miles Inc., USA) and frozen with a mixture of acetone and dry ice (–80°C). The frozen samples were sliced to 30 μm thickness in the cryostat (Carl Zeiss, Germany) at –20°C, and were mounted on glass slides and air-dried. The sections were exposed to an imaging plate at –20°C for 90 min to produce ^{18}F-FMT images. The same sections were exposed to another imaging plate again for 7 days to generate ^{14}C-DG images, 4 days after the first exposure. Autoradiograms were digitized using the Bio-Imaging Analyzer.

Regions of interest (ROIs) were drawn along the margins of the tissues in the ^{14}C-DG image. The same ROIs were applied to the ^{18}F-FMT image. The photo-stimulated luminescence of each image was transformed to the relative radioactivity using software (BAStation, Fuji Photo Film Co., Ltd., Japan). The ratios of relative activity in tissue/muscle and tumor/inflammation were calculated.

Statistical analysis

One-way ANOVA with Scheffé's F correction was used to analyze all the results. Statistical significance was considered at $p < 0.05$.

RESULTS

Histological examination of inflammatory tissues

Histology of Day 4 aseptic inflammatory tissues revealed

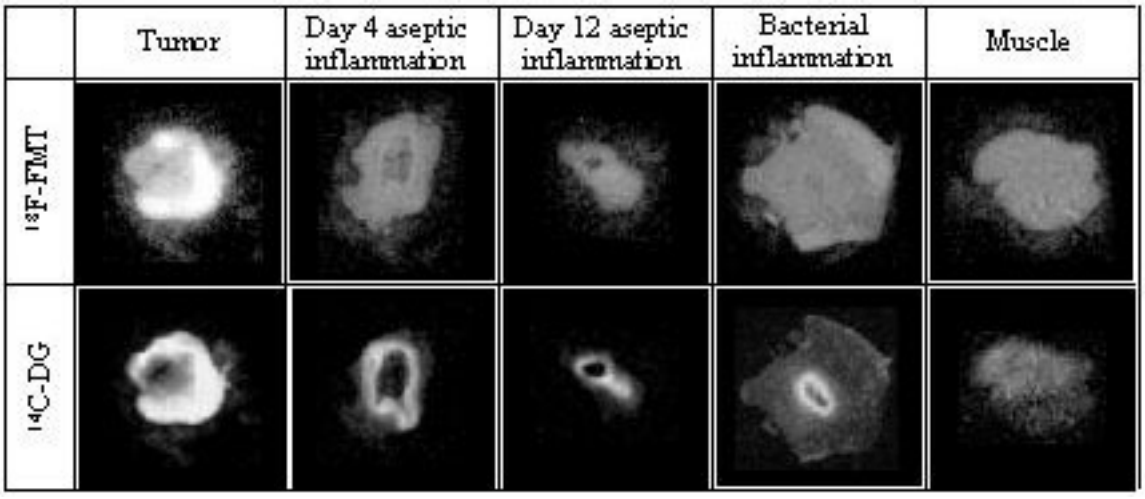

Fig. 2 Dual tracer macro autoradiograms of a rat bearing AH109A tumor and aseptic and bacterial inflammation. The ^{18}F-FMT images (*upper picture*) and ^{14}C-DG images (*lower picture*) are shown.

Table 2 Radioactivity ratios of tissue to muscle and tumor to inflammation in dual tracer macro autoradiographic study

Tissue	Tissue/muscle ratio Tumor/inflammation ratio	
	^{18}F-FMT	^{14}C-DG
Tumor	3.41 ± 0.67	13.19 ± 1.72
Day 4 aseptic	1.17 ± 0.26	7.63 ± 1.95
inflammation	3.01 ± 0.62	1.18 ± 0.43
Day 12 aseptic	1.25 ± 0.20	5.84 ± 1.72
inflammation	2.78 ± 0.41	2.41 ± 0.64
Bacterial	1.13 ± 0.17	5.20 ± 0.30
inflammation	3.09 ± 0.45	2.54 ± 0.15

Values are expressed as mean ± S.D. (n = 5)

an inflammatory cell layer and granulation tissue around the injected oil, compatible with the chronic phase of inflammation. The histology of Day 12 aseptic inflammatory tissue showed almost the same findings, although the number of inflammatory cells was less than that on Day 4, indicating the healing stage of inflammation. Similar inflammatory reactions were identified around the central necrosis in the case of bacterial inflammation.

Biodistribution of ^{18}F-FMT

Table 1 summarizes the results of biodistribution studies for ^{18}F-FMT in rats bearing tumor and inflammation. The radioactivity in the blood gradually decreased with time from 0.63%ID/g at 5 min after injection. Tissue radioactivity in most organs including the liver and kidney, but except the pancreas, brain and bone, was as low as in blood and similarly decreased with time. The radioactivity in the pancreas was the highest and relatively constant during 120 min of measurement. The radioactivity in the bone and urine increased gradually during the experiment. The tumor uptake of ^{18}F-FMT increased with time, reaching a peak at 60 min after injection (1.43%ID/g) and decreased thereafter. The tumor uptakes at 30 and 60 min were significantly higher than those of the other tissues except the pancreas. The uptakes both in aseptic and bacterial inflammation were very low throughout the experiments.

Whole-body autoradiographic study with ^{18}F-FMT and ^{14}C-DG

Figure 1 shows whole-body autoradiograms obtained at 60 min after dual injection of ^{18}F-FMT and ^{14}C-DG. In the ^{18}F-FMT image, high radioactivity was observed in the tumor and pancreas, while it was very low in the two aseptic inflammatory tissues. Relatively high radioactivity was observed in bone cortex. In ^{14}C-DG image, high radioactivity was observed both in tumor and inflammation. Very high radioactivity was observed in the Day 4 inflammation at the rim of the inoculated oil, while this high uptake decreased in Day 12 inflammation.

Macro autoradiographic study with ^{18}F-FMT and ^{14}C-DG

Figure 2 shows representative macro autoradiograms of tumor, aseptic and bacterial inflammatory tissues and the muscle at 60 min after injection of ^{18}F-FMT and ^{14}C-DG. ^{18}F images, clearly indicated that tumor uptake of ^{18}F-FMT was higher than the other tissues, while the accumulations in aseptic and bacterial inflammatory tissues were almost equal to that of the muscle. ^{14}C-DG images show high accumulations in aseptic and bacterial inflammatory tissues as well as in tumor.

Table 2 summarizes the radioactivity ratios of tissue-to-muscle and tumor-to-inflammation computed from dual tracer macro autoradiograms at 60 min after injection. The ^{18}F radioactivity in the tumor was significantly

higher than that of the muscle and inflammation ($p < 0.01$). The ^{14}C radioactivity in tumor and aseptic and bacterial inflammation was higher than that of muscle significantly ($p < 0.01$). Tumor-to-inflammation ratios of ^{18}F-FMT were higher than those of ^{14}C-DG in every inflammation.

DISCUSSION

The purpose of this study was to evaluate the potential efficacy of ^{18}F-FMT, a new tumor imaging agent, for differentiation between tumor and inflammation. Our results indicated that the accumulation of ^{18}F-FMT in tumor was significantly higher than those in other tissues ($p < 0.01$), except the pancreas. ^{18}F-FMT accumulation both in aseptic and bacterial inflammation was not marked and was similar to the muscle and other background tissues. Consequently, ^{18}F-FMT is a promising tracer for the differentiation between tumor and inflammation.

Ishiwata et al. reported the tissue distribution of ^{18}F-FMT and the high accumulation in tumor, using Donryu rats bearing AH109A hepatoma.[26] We obtained the similar results in this study, using the same tumor cell line. The biodistribution study showed increasing radioactivity in the bone, and the whole-body autoradiogram with ^{18}F-FMT disclosed relatively high radioactivity in the cortical bone and low radioactivity in the bone marrow. These findings might be explained by uptake of ^{18}F ion from defluorination of ^{18}F-FMT *in vivo*. It was reported that small amounts of ^{18}F-fluorinated metabolites existed in the plasma and tumor after injection of ^{18}F-FMT by thin-layer chromatography.[26] The accumulation of radioactivity in the urine increased with time in this study. This finding would be related to the PET image findings reported by Ishiwata et al., in which relatively high hot spots were observed on the bladder 30 and 60 min after injection of ^{18}F-FMT.

Tissue distribution of ^{18}F-FMT was comparable to those of other tyrosine analogs such as ^{18}F-FET and L-3-[^{18}F]fluoro-α-methyl tyrosine, while ^{18}F-FMT has the following advantages. Tumor to normal tissue radioactivity ratios of ^{18}F-FMT were higher than those of ^{18}F-FET, although the animal models were different.[19–21] The most notable difference between ^{18}F-FMT and L-3-[^{18}F]fluoro-α-methyl tyrosine was the accumulation in the kidney. The accumulation of ^{18}F-FMT in the kidney was in the blood level, whereas L-3-[^{18}F]fluoro-α-methyl tyrosine accumulated greatly in the kidney like in the pancreas.[22,23] ^{18}F-FMT accumulation in the liver was very low, similar to other synthetic amino acid tracers such as ^{18}F-FET[19–21] and L-3-[^{18}F]fluoro-α-methyl tyrosine.[22,23] On the other hand, analogues of natural amino acid tracers such as L-[2-^{18}F]fluorotyrosine[11] and L-methyl-^{11}C-methionine[16] accumulated highly in the liver. These properties of ^{18}F-FMT suggested that ^{18}F-FMT is a promising candidate as a tumor-detecting agent in the abdominal region except for the pancreas.

The aseptic inflammation induced by turpentine oil followed the models used by Yamada et al.[27] They demonstrated that the accumulation of ^{18}F-FDG in this type of inflammation peaked at 4 days after inoculation of the turpentine oil and then decreased gradually from 7 to 14 days after inoculation. They also showed by micro-autoradiography that high radioactivity areas corresponded to inflammatory cell layers and granulation tissue. Therefore, the high ^{14}C-DG radioactivity regions in the inflammatory tissues in this study should correspond to the inflammatory cell layer and granulation tissues as confirmed by the histological examination. We took two time points for the turpentine oil induced inflammation models. The Day 4 and Day 12 represent the intense and decreasing phases respectively of the ^{18}F-FDG accumulation in the chronic inflammatory phase.

Kaim et al. evaluated the accumulation of ^{18}F-FDG in the abscess induced by *S. aureus*, as a bacterial inflammatory model by macro autoradiography.[4] They demonstrated that inflammatory cell layers and granulation tissues within the abscesses 2 and 5 days after inoculation showed an increasing pattern in ^{18}F-FDG accumulation. We could confirm this tendency using ^{14}C-DG. It was reported that the inflammation induced by *S. aureus* took little ^{18}F-FET.[28] The accumulation of ^{18}F-FMT in bacterial inflammation was similarly low in the present study. Therefore, both the ^{18}F-FMT and ^{18}F-FET would be equally useful for the differentiation between tumor and bacterial inflammation.

We used ^{14}C-DG instead of ^{18}F-FDG to assess tissue glucose metabolism in this study. Since the metabolism is almost identical between ^{14}C-DG and ^{18}F-FDG,[29] the results of this study would apply to ^{18}F-FDG. It appears that ^{18}F-FMT is more specific to tumor than ^{14}C-DG, although the relative uptake of ^{18}F-FMT in tumor is less than that of ^{14}C-DG. ^{18}F-FMT will be a tracer of choice to characterize lesions, while ^{18}F-FDG would be more suitable to pick up lesions either malignant or inflammatory.

^{11}C-Met is the most frequently used radiolabeled amino acid because of its rapid synthesis with high radiochemical yield.[31] However, the half-life of carbon-11, 20 min, limits its availability. The longer half-life of fluorine-18 would be more suitable for whole-body PET scans and future radiopharmaceutical deliveries to PET centers without an on-site cyclotron. Especially, ^{18}F-FMT is suitable for routine production, because of the simple preparation, high production yield and easy automation for synthetic procedure.[25] These features are advantages in the clinical application of ^{18}F-FMT.

In conclusion, although this study is still preliminary, ^{18}F-FMT seems promising for the differentiation between tumor and inflammation because of higher specificity to tumor than ^{14}C-DG. The simple preparation of ^{18}F-FMT with high radiochemical yields supports routine production for clinical PET practice in oncology.

ACKNOWLEDGMENTS

This study was supported by Future Medical Engineering Based on Bio-nanotechnology Tohoku University 21st Century Center of Excellence Program. We appreciate the technical support of Mr. Y. Sugawara at the Institute of Development, Aging and Cancer, Tohoku University and all the members of the Cyclotron and Radioisotope Center, Tohoku University.

REFERENCES

1. Brock CS, Meikle SR, Price P. Does fluorine-18 fluorodeoxyglucose metabolic imaging of tumours benefit oncology? *Eur J Nucl Med* 1997; 24: 691–705.
2. Rigo P, Paulus P, Kaschten BJ, Hustinx R, Bury T, Jerusalem G, et al. Oncological applications of positron emission tomography with fluorine-18 fluorodeoxyglucose. *Eur J Nucl Med* 1996; 23: 1641–1674.
3. Ishimori T, Saga T, Mamede M, Kobayashi H, Higashi T, Nakamoto Y, et al. Increased ^{18}F-FDG uptake in a model of inflammation: concanavalin A-mediated lymphocyte activation. *J Nucl Med* 2002; 43: 658–663.
4. Achim HK, Bruno W, Michael OK, Jochen G, Gustav KS, Alfred B. Autoradiographic quantification of ^{18}F-FDG uptake in experimental soft-tissue abscesses in rats. *Radiology* 2002; 223: 446–451.
5. Kubota R, Kubota K, Yamada S, Tada M, Ido T, Tamahashi N. Microautoradiographic study for the differentiation of intratumoral macrophages, granulation tissues and cancer cells by the dynamics of fluorine-18-fluorodeoxyglucose uptake. *J Nucl Med* 1994; 35: 104–112.
6. Kubota R, Yamada S, Kubota K, Ishiwata K, Tamahashi N, Ido T. Intratumoral distribution of fluorine-18-fluorodeoxyglucose *in vivo*: high accumulation in macrophages and granulation tissues studied by microautoradiography. *J Nucl Med* 1992; 33: 1972–1980.
7. Strauss LG. Fluorine-18 deoxyglucose and false-positive results: a major problem in the diagnostics of oncological patients. *Eur J Nucl Med* 1996; 23: 1409–1415.
8. Hustinx R, Smith RJ, Benard F, Rosenthal DI, Machtay M, Farber LA, et al. Dual time point fluorine-18 fluorodeoxyglucose positron emission tomography: a potential method to differentiate malignancy from inflammation and normal tissue in the head and neck. *Eur J Nucl Med* 1999; 26: 1345–1348.
9. Kubota K, Itoh M, Ozaki K, Ono S, Tashiro M, Yamaguchi K, et al. Advantage of delayed whole-body FDG-PET imaging for tumour detection. *Eur J Nucl Med* 2001; 28: 696–703.
10. Zhao S, Kuge Y, Tsukamoto E, Mochizuki T, Kato T, Hikosaka K, et al. Effects of insulin and glucose loading on FDG uptake in experimental malignant tumours and inflammatory lesions. *Eur J Nucl Med* 2001; 28: 730–735.
11. Ishiwata K, Kubota K, Murakami M, Kubota R, Sasaki T, Ishii S, et al. Re-evaluation of amino acid PET studies: can the protein synthesis rates in brain and tumor tissues be measured *in vivo*? *J Nucl Med* 1993; 34: 1936–1943.
12. Isselbacher KJ. Sugar and amino acid transport by cells in culture-differences between normal and malignant cells. *N Engl J Med* 1972; 286: 929–933.
13. Isselbacher KJ. Increased uptake of amino acids and 2-deoxy-D-glucose by virus-transformed cells in culture. *Proc Natl Acad Sci USA* 1972; 69: 585–589.
14. Kubota R, Kubota K, Yamada S, Tada M, Takahashi T, Iwata R, et al. Methionine uptake by tumor tissue: a microautoradiographic comparison with FDG. *J Nucl Med* 1995; 36: 484–492.
15. Kubota K, Kubota R, Yamada S, Tada M. Effects of radiotherapy on the cellular uptake of carbon-14 labeled L-methionine in tumor tissue. *Nucl Med Biol* 1995; 22: 193–198.
16. Kubota K, Matsuzawa T, Fujiwara T, Sato T, Tada M, Ido T, et al. Differential diagnosis of AH109A tumor and inflammation by radioscintigraphy with L-[methyl-^{11}C]methionine. *Jpn J Cancer Res* 1989; 80: 778–782.
17. Laverman P, Boerman OC, Corstens FH, Oyen WJ. Fluorinated amino acids for tumour imaging with positron emission tomography. *Eur J Nucl Med* 2002; 29: 681–690.
18. Jager PL, Vaalburg W, Pruim J, de Vries EG, Langen KJ, Piers DA. Radiolabeled amino acids: basic aspects and clinical applications in oncology. *J Nucl Med* 2001; 42: 432–445.
19. Tang G, Wang M, Tang X, Luo L, Gan M. Pharmacokinetics and radiation dosimetry estimation of *O*-(2-[^{18}F]fluoroethyl)-L-tyrosine as oncologic PET tracer. *Appl Radiat Isot* 2003; 58: 219–225.
20. Heiss P, Mayer S, Herz M, Wester HJ, Schwaiger M, Senekowitsch-Schmidtke R. Investigation of transport mechanism and uptake kinetics of *O*-(2-[^{18}F]fluoroethyl)-L-tyrosine *in vitro* and *in vivo*. *J Nucl Med* 1999; 40: 1367–1373.
21. Wester HJ, Herz M, Weber W, Heiss P, Senekowitsch-Schmidtke R, Schwaiger M, et al. Synthesis and radiopharmacology of *O*-(2-[^{18}F]fluoroethyl)-L-tyrosine for tumor imaging. *J Nucl Med* 1999; 40: 205–212.
22. Amano S, Inoue T, Tomiyoshi K, Ando T, Endo K. *In vivo* comparison of PET and SPECT radiopharmaceuticals in detecting breast cancer. *J Nucl Med* 1998; 39: 1424–1427.
23. Inoue T, Tomiyoshi K, Higuichi T, Ahmed K, Sarwar M, Aoyagi K, et al. Biodistribution studies on L-3-[fluorine-18]fluoro-α-methyl tyrosine: a potential tumor-detecting agent. *J Nucl Med* 1998; 39: 663–667.
24. Coenen HH, Kling P, Stocklin G. Cerebral metabolism of L-[2-^{18}F]fluorotyrosine, a new PET tracer of protein synthesis. *J Nucl Med* 1989; 30: 1367–1372.
25. Iwata R, Furumoto S, Pascali C, Bogni A, Ishiwata K. Radiosynthesis of *O*-[^{11}C]methyl-L-tyrosine and *O*-[^{18}F]fluoromethyl-L-tyrosine as potential PET tracers for imaging amino acid transport. *J Label Compd Radiopharm* 2003; 46: 555–566.
26. Ishiwata K, Kawamura K, Wang WF, Furumoto S, Kubota K, Pascali C, et al. Evaluation of *O*-[^{11}C]methyl-L-tyrosine and *O*-[^{18}F]fluoromethyl-L-tyrosine as tumor imaging tracers by PET. *Nucl Med Biol* 2004; 31: 191–198.
27. Yamada S, Kubota K, Kubota R, Ido T, Tamahashi N. High accumulation of fluorine 18-fluorodeoxyglucose in turpentine-induced inflammatory tissue. *J Nucl Med* 1995; 36: 1301–1306.
28. Kaim AH, Weber B, Kurrer MO, Westera G, Schweitzer A, Gottschalk J, et al. ^{18}F-FDG and ^{18}F-FET uptake in experimental soft tissue infection. *Eur J Nucl Med* 2002; 29: 648–654.

29. Fowler JS, Ido T. Design and synthesis of 2-deoxy-2-[^{18}F]fluoro-D-glucose (^{18}FDG). In: *Handbook of Radiopharmaceuticals*, Welch MJ, Redvanly CS (eds), England; John Wiley & Sons Inc., 2003: 307–322.

30. Langstrom B, Antoni G, Gullberg P, Halldin C, Malmborg P, Nagren K, et al. Synthesis of L- and D-[methyl-^{11}C]methionine. *J Nucl Med* 1987; 28: 1037–1040.